

A Spatial Autoregressive Graphical Model with Applications in Intercropping

Sjoerd Hermes^{1,2}, Joost van Heerwaarden^{1,2} and Pariya Behrouzi¹

¹ Mathematical and Statistical Methods, Wageningen University

² Plant Production Systems, Wageningen University

Abstract

Within the statistical literature, there is a lack of methods that allow for asymmetric multivariate spatial effects to model relations underlying complex spatial phenomena. Intercropping is one such phenomenon. In this ancient agricultural practice multiple crop species or varieties are cultivated together in close proximity and are subject to mutual competition. To properly analyse such a system, it is necessary to account for both within- and between-plot effects, where between-plot effects are asymmetric. Building on the multivariate spatial autoregressive model and the Gaussian graphical model, the proposed method takes asymmetric spatial relations into account, thereby removing some of the limiting factors of spatial analyses and giving researchers a better indication of the existence and extend of spatial relationships. Using a Bayesian-estimation framework, the model shows promising results in the simulation study. The model is applied on intercropping data consisting of Belgian endive and beetroot, illustrating the usage of the proposed methodology. An R package containing the proposed methodology can be found on <https://CRAN.R-project.org/package=SAGM>.

Keywords: Graphical models; spatial autoregressive models; asymmetric effects; intercropping.

1 Introduction

Gaussian graphical models are statistical learning techniques used to make inference on conditional dependence relationships within a set of variables arising from a multivariate normal distribution (Lauritzen, 1996). Methodological developments have expanded the use of the Gaussian graphical model beyond static (non-temporal) to dynamic (temporal) data, through, for example, the use of time-varying or autoregressive graph structures (see for relevant research during the last 5 years Barigozzi & Brownlees, 2019; Paci & Consonni, 2020; Yang & Peng, 2020; Dallakyan et al., 2022). These developments allow for improved analyses of complex, multivariate temporal datasets. However, barely any attention has been given to the development of graphical models pertaining to the higher dimensional cousin of time: space. Where dynamic models deal with temporal variation, assuming data close in time (Yang & Peng, 2020), there are clear parallels with the spatial analogue, for which data close together in space can be expected to be similar due to potential presence of location-specific latent factors affecting the distributions of the data that pertain to the location.

One example of spatial dependence between different variables can be found in intercropping trials. Intercropping is the cultivation of multiple crop species in a single field. This practice is particularly common in smallholder farming in the Global South, where it helps mitigate different types of production risk (Fordham, 1983). However, intercropping has other potential benefits over monocropping, such as increased yield, reduced inputs, improved soil and water quality, carbon sequestration, and biodiversity conservation (Maitra et al., 2021; Li et al., 2023). These benefits generally derive from synergy among neighbouring crops, such as caused by nitrogen fixation and transfer by legumes (Stern, 1993; Chu et al., 2004) or by spatial and temporal complementarity below and above ground (Yang et al., 2017; Zhang et al., 2017; Homulle et al., 2021).

Certain traits of the crops, such as yield, are not only dependent on within-crop processes, but also depend on the effects of traits expressed by different crops growing on neighbouring plots. These effects can be either positive (complementarity and facilitation) or negative (competition) (Bourke et al., 2021) with respect to biomass production and yield. Knowledge of such effects is invaluable in selecting intercropping combinations with the goal of yield-maximization (Bourke et al., 2021). Contemporary research on intercropping systems has shown that these spatial effects exhibit asymmetry (Huang et al., 2017; Gao et al., 2021), that is, the effect of variables pertaining to crop c on variables pertaining to crop c' is not the same as the effect of those same variables pertaining to crop c' on those of crop c .

Despite a growing interest in the design of productive intercropping systems (Federer 2012), there has been

little methodological development around the identification of the kind of multi-trait and multi-species interactions that would determine which crops should ideally be combined (Brooker et al., 2015). Given that intercropping data typically consist of observations on locations in a finite domain, the set of spatial autoregressive models (Ord, 1975) makes for a logical starting point in this methodological pursuit. An application of this model on yield data in a monocropping system can be found in Long (1998). Whilst being suitable for data arising from monocropping systems, this approach is unsuitable for modern intercropping type data that consist of multiple traits measured across multiple crops, as the spatial autoregressive model is univariate in its response and has no way of isolating asymmetric spatial effects or within-plot effects. Another example of an existing approach, by Dobra (2011; 2016), explicitly accounts for spatial autocorrelation by developing Bayesian models that construct two graphs: a neighbourhood graph where the vertices indicate different regions and the presence of an edge indicates whether the regions share a border (are neighbours), and a conditional dependence graph that shows which variables are independent given all other variables. However, this approach has no way of inferring the spatial effects of one variable of crop c on another of crop c' , which is of interest to researchers wanting to evaluate, for example, the impact of applying fertiliser on one plot on the growth of plants in surrounding plots. Whilst other spatial (autoregressive) models exist, none can model heterogenous spatial effects for multiple crops, of which multiple traits are evaluated, whilst simultaneously capturing the complex dependence relations that occur within plots.

In line with Dahlhaus and Eichler (2003), who proposed a time series (VAR) chain graph, showcasing contemporaneous conditional dependencies and dynamic effects, we propose a spatial autoregressive graphical model that fills this methodological gap. Our proposed spatial autoregressive graphical model builds on the recently proposed multivariate spatial autoregressive model (MSAR) by Yang and Lee (2017), who extended the univariate spatial autoregressive model (SAR) to the multivariate setting. The asymmetry of spatial effects between different crops is captured through a straightforward manipulation of the spatial weight matrices of the MSAR model, whilst the within-plot dependencies share some of the properties of the Gaussian graphical model; namely that the within-plot effects are derived from an underlying network consisting of conditional dependencies, which, in turn, offer a parsimonious representation of the complex within-plot dependencies as well as being easily interpretable for researchers. The proposed method has attractive between-location independence relationships, that are rarely present in spatial autoregressive models. Using this approach, we can identify positive and negative interaction effects between crops that optimise collective performance, thereby selecting combinations of genotypes or crops that are promising in intercropping situations.

We propose a Bayesian estimation framework and introduce an R package such that researchers can analyse their own intercropping data. The R package can be found at <https://CRAN.R-project.org/package=SAGM>.

This article proposes a new statistical methodology: the spatial autoregressive graphical model. The methodological novelty arises from the method's capacity to learn multivariate asymmetric between-location effects, combined with the capacity of illustrating complex within-location effects through a conditional independence structure, whereby the between- and within-location effects are illustrated by means of a graph, thereby facilitating interpretability. Section 2, introduces and formalises the methodological framework. Bayesian inference is discussed in Section 3. Section 4 presents an elaborate simulation study, where the performance of the newly proposed method is evaluated on a simulated spatial dataset. An application of the new method on real intercropping data, illustrating the usage of the proposed methodology, is given in Section 5. Finally, the conclusion and discussion can be found in Section 6.

2 Methodology

2.1 Spatial autoregressive models

The proposed methodology requires some background knowledge about the MSAR model. Assume data arising from a stochastic process $\{X(i) : i = 1, \dots, n\}$, with $\bigcup_{i=1}^n i = \mathcal{D}$ and $i \cap i' = \emptyset$ for all $i \neq i'$. Ergo: the data are lattice data, where the lattice \mathcal{D} is a non-random and finite domain. The different locations i will represent plots containing multiple plants of a single crop. The MSAR (Yang & Lee, 2017) is given by the following equation

$$\mathbf{X} = \mathbf{W} \mathbf{X} \boldsymbol{\Psi} + \mathbf{E}, \quad (1)$$

with $\mathbf{X} \in \mathbb{R}^{n \times p}$, $\mathbf{W} \in \mathcal{Z}^{n \times n}$, where $\mathcal{Z} = \{x \in \mathbb{R} | 0 \leq x \leq 1\}$, $\boldsymbol{\Psi} \in \mathbb{R}^{p \times p}$ and $\mathbf{E} \in \mathbb{R}^{n \times p}$ and where the row vectors of $\mathbf{E} = (\mathbf{E}_1, \dots, \mathbf{E}_n)^T$, $\mathbf{E}_i = (\varepsilon_{i1}, \dots, \varepsilon_{ip})$, $1 \leq i \leq n$, are assumed to be i.i.d. normally distributed with mean vector $\mathbf{0}$ and positive definite covariance matrix $\boldsymbol{\Sigma}_E$. \mathbf{W} is a known spatial weight matrix and $\boldsymbol{\Psi}$ indicates how variables in one plot affects the value of variables in neighbouring plots and vice versa.

To understand the concept of spatial weight matrices, an introduction to the adjacency matrix \mathbf{A} is necessary, as \mathbf{A} determines the structure of the spatial weight matrix \mathbf{W} . Element $a_{ij} = a_{ji} = 1$, $1 \leq i \neq j \leq n$, if location i is neighboured by location j and 0 otherwise. Moreover, $a_{ii} = 0$ for all i . \mathbf{W} is a row-normalised version of \mathbf{A} ,

i.e. $w_{ij} = \frac{a_{ij}}{|\{i\} \neq \emptyset|}$, where $|\cdot|$ denotes the cardinality of a set. Therefore, $(\mathbf{W}\mathbf{X})_{i\cdot}$ contains the average for each variable over the neighbours of location i .

2.2 Accounting for between-crop heterogeneity and asymmetric effects

When multiple crop species are grown in conjunction with one another, researchers might want to evaluate the effects of one crop on another. When these are two distinct crops, symmetric spatial effects become unlikely (Huang et al., 2017; Gao et al., 2021), due to, for example, shade cast on the shorter crop by the leaves of the taller crop. To account for this ecological heterogeneity in structural parameters, the model proposed in (1) can be extended as

$$\mathbf{X} = \mathbf{W}_{c',c}\mathbf{X}\Psi_{c',c} + \mathbf{W}_{c,c'}\mathbf{X}\Psi_{c,c'} + \mathbf{E} \quad (2)$$

where $\Psi_{c',c} \in \mathbb{R}^{p \times p}$ contains the effect of each trait of crop c' on each trait of crop c and $\Psi_{c,c'} \in \mathbb{R}^{p \times p}$ contains the effect of each trait of crop c on each trait of crop c' . Spatial weight matrices $\mathbf{W}_{c',c} \in \mathcal{Z}^{n \times n}$ and $\mathbf{W}_{c,c'} \in \mathcal{Z}^{n \times n}$ are chosen such that only the matrix elements pertaining to direct neighbouring plots of respectively crop c and c' containing respectively crop c' and c are nonzero. Vectorising (2) leads to the data generating process $\text{vec}(\mathbf{X}) = \left(\mathbf{I}_{np} - \sum_{k=1}^2 \Psi_k^T \otimes \mathbf{W}_k\right)^{-1} \text{vec}(\mathbf{E})$ consisting of an $np \times np$ identity matrix \mathbf{I}_{np} , where, for readability and generality, k is used to denote the crop ordering.

Definition 1. (*Spatial weight matrix structure*) Given two neighbouring crops c and c' , the adjacency matrix $\mathbf{A}_{c',c}$ isolating the observations of crop c' with neighbour crop c is of the following form:

$$a_{(ij),c',c} \begin{cases} 1, & \text{if plot } i \text{ contains crop } c \text{ and plot } j \text{ contains crop } c' \\ 0, & \text{otherwise.} \end{cases}$$

Subsequently, $\mathbf{W}_{c',c}$ contains elements $w_{(ij),c',c} = \frac{a_{(ij),c',c}}{|\{a_{(i),c',c} \neq 0\}|}$.

Using this formulation, whilst it might seem feasible to extend the model to experiments where more than two crops are planted in field trials containing random neighbours, the model becomes unidentifiable, see Section 2.5. Therefore, we will restrict analyses to scenarios consisting of 2 crops.

For stability reasons, i.e. ensuring a positive Jacobian term in the likelihood, spatial autoregressive models typically impose restrictions on the values that the spatial autoregressive parameter can take. Our method is no different in this regard.

Assumption 1. (*Stability condition*) To estimate the spatial effects, we require that $\det\left(\mathbf{I}_{np} - \sum_{k=1}^2 \Psi_k^T \otimes \mathbf{W}_k\right) > 0$, which is guaranteed whenever $\lambda_{\min}\left(\sum_{k=1}^2 \Psi_k^T \otimes \mathbf{W}_k\right) > -1$ and $\lambda_{\max}\left(\sum_{k=1}^2 \Psi_k^T \otimes \mathbf{W}_k\right) < 1$, where $\lambda_{\min}(\cdot)$ and $\lambda_{\max}(\cdot)$ are the minimum and maximum eigenvalues respectively, is a sufficient condition.

In addition to the spatial effects contained in the Ψ_k , our interest lies in the within-plot effects, contained in $\Theta_E = \Sigma_E^{-1}$, the precision matrix of \mathbf{E} . In order to obtain these within-plot effects, a so-called spatial filter is required. The model specification in (2) allows for the construction of such a filter $\mathbf{R}(\Psi)\text{vec}(\mathbf{X}) = \text{vec}(\mathbf{E})$, where $\mathbf{R}(\Psi) = \left(\mathbf{I}_{np} - \sum_{k=1}^2 \Psi_k^T \otimes \mathbf{W}_k\right)$ is the spatial filter matrix, filtering out the spatial effects on the observations as $\text{vec}(\mathbf{X}) - \left(\sum_{k=1}^2 \Psi_k^T \otimes \mathbf{W}_k\right) \text{vec}(\mathbf{X}) = \text{vec}(\mathbf{E})$, resulting in the within-plot data, under the assumption that all spatial dependencies are accurately captured by the \mathbf{W}_k (Getis, 1990; Millo, 2014).

On a related note, as \mathbf{X} is a linear combination of Gaussian variables, \mathbf{X} itself is Gaussian with the following expected value

$$\begin{aligned} \mathbb{E}[\text{vec}(\mathbf{X})] &= \mathbb{E}[\mathbf{R}(\Psi)\text{vec}(\mathbf{E})] \\ &= \mathbf{R}(\Psi)\mathbb{E}[\text{vec}(\mathbf{E})] \\ &= \mathbf{0}. \end{aligned}$$

and variance

$$\begin{aligned} \text{Var}[\text{vec}(\mathbf{X})] &= \mathbb{E}[\text{vec}(\mathbf{X})\text{vec}(\mathbf{X})^T] \\ &= \mathbb{E}\left\{\left[\mathbf{R}(\Psi)^{-1}\text{vec}(\mathbf{E})\right]\left[\mathbf{R}(\Psi)^{-1}\text{vec}(\mathbf{E})\right]^T\right\} \\ &= \mathbf{R}(\Psi)^{-1}(\Sigma_E \otimes \mathbf{I}_n)\mathbf{R}(\Psi)^{-T}. \end{aligned}$$

Consequently, $\text{vec}(\mathbf{X})$ is distributed as $\text{vec}(\mathbf{X}) \sim N_{np}(\mathbf{0}, \mathbf{R}(\Psi)^{-1}(\Sigma_E \otimes \mathbf{I}_n)\mathbf{R}(\Psi)^{-T})$, shortened as $\text{vec}(\mathbf{X}) \sim N_{np}(\mathbf{0}, \Sigma_X)$. The resulting $\Sigma_X = \Theta_X^{-1}$ matrix is a $np \times np$ block matrix, where each block contains the variances or covariances within and between crops. Θ_E consists of the original conditional dependences within a plot, prior to being affected by any spatial processes. As the spatial effects also distort the conditional dependencies

within a plot, evaluating the within-plot elements of Θ_X is inadequate. In essence, our interest lies in the true underlying conditional dependencies found in Θ_E , even though we only have data after the occurrence of spatial effects. By separating these effects, the true within-crop dependencies can be obtained. As such, there is an equivalence between Θ_E , containing the within-plot interactions, and the precision matrix corresponding to the time series chain graph (Dahlhaus & Eichler 2003; Abegaz & Wit, 2013), which contains the contemporaneous interactions, in addition to establishing the connection to the Gaussian graphical model.

2.3 Graphical model

Gaussian graphical models are multivariate statistical models that use graphs $G = (V, E)$ to represent the full conditional dependence structure between variables represented by a set of vertices $V = \{1, 2, \dots, p\}$ through the use of a set of undirected edges $E \subset V \times V$, and depends on a $n \times p$ data matrix $\mathbf{X} = (\mathbf{X}_1, \mathbf{X}_2, \dots, \mathbf{X}_p)$, $\mathbf{X}_j = (X_{1j}, X_{2j}, \dots, X_{nj})^T$, $j = 1, \dots, p$, where the n row vectors in \mathbf{X} are independent and identically distributed according to $N_p(\mathbf{0}, \Theta^{-1})$. Θ contains the scaled partial correlations: $\rho_{ij} = -\frac{\theta_{ij}}{\sqrt{\theta_{ii}\theta_{jj}}}$. Thus, the partial correlation ρ_{ij} represents the independence between \mathbf{X}_i and \mathbf{X}_j conditional on $\mathbf{X}_{V \setminus ij}$. Therefore, $(i, j) \notin E \Leftrightarrow \rho_{ij} = 0$.

The spatial autoregressive graphical model is a special type of Gaussian graphical model consisting of both directed and undirected edges. This graphical model captures the complex dependency structure of the data in a parsimonious and well-interpretable manner. To formalise this notion, a few definitions are introduced.

Definition 2. (*Within-plot effect graph*) The within-plot graph corresponding to \mathbf{X} is an undirected graph $G_w = (V, E_w)$ with edge set E_w such that

$$(i-j) \notin E_w \Leftrightarrow \theta_{Eij} = \theta_{Eji} = 0, \quad 1 \leq i \neq j \leq p.$$

Definition 3. (*Between-plot effect graph*) The between-plot effect graph corresponding to \mathbf{X} is a directed graph $G_{b:c,c'} = (V_c \cup V_{c'}, E_{b:c,c'} \cup E_{b:c',c}) = G_{b:c',c}$, where $c' \in \mathcal{N}_c$, with \mathcal{N}_c denoting the set of crops neighboured to crop c , and with edge set $E_{b:c,c'} \cup E_{b:c',c}$ such that

$$\begin{aligned} (i \rightarrow j) \notin E_{b:c,c'} &\Leftrightarrow \psi_{c,c',ij} = 0, \quad (j \rightarrow i) \notin E_{b:c,c'} \Leftrightarrow \psi_{c,c',ji} = 0, \\ (i \rightarrow j) \notin E_{b:c',c} &\Leftrightarrow \psi_{c',c,ij} = 0, \quad (j \rightarrow i) \notin E_{b:c',c} \Leftrightarrow \psi_{c',c,ji} = 0. \end{aligned}$$

Therefore, $E_{b:c,c'}$ represents the set of all directed edges from crop c to crop c' and $E_{b:c',c}$ represents the set of all directed edges from crop c' to crop c .

From Definition 2 we note that θ_{Eij} is the scaled partial correlation between variables i and j for any plot and Definition 3 shows that $\psi_{c,c',ij}$ is the effect of variable i of crop c on the value of variable j of crop c' . Unfortunately, whereas the directed edges of the approach by Dahlhaus and Eichler (2003) reflect Granger causality, the directed edges for the proposed method do not. This is because there exists no spatial analogue to Granger causality, as spatial ordering is not one-dimensional, and one can move back and forth between plots.

By combining Definitions 2 and 3, a spatial chain graph is obtained that contains the full between- and within-plot dependency structure.

Definition 4. (*Spatial chain graph*) The spatial chain graph corresponding to \mathbf{X} is a partially directed graph $G_s = (V_s, E_s) = (V_c \cup V_{c'}, E_{b:c,c'} \cup E_{b:c',c} \cup E_w)$ with edge set $E_{b:c,c'} \cup E_{b:c',c} \cup E_w$ as defined in Definitions 2 and 3 respectively. Thus, for $c' \in \mathcal{N}_c$, there exists a directed edge from $V_{i,c}$ to $V_{j,c'}$ if and only if $(i \rightarrow j) \in E_{b:c,c'}$, $1 \leq i \neq j \leq p$. Moreover, for any crop c , there exists an undirected edge between $V_{i,c}$ and $V_{j,c}$ if and only if $(i-j) \in E_w$.

2.4 Independence relations

A graphical model for a set of variables is defined as a model where the conditional dependence relations specified by the model are given by a graph. Accordingly, a graphical model goes beyond the visualisation of relationships found in data. This also holds for the spatial autoregressive graphical model, where a distinction should be made between two types of dependence relations: within- and between-crop dependencies. Accordingly, this section will cover both type of dependencies and illustrate how they hold for the proposed method.

Theorem 1. (*Within-crop conditional independence*) Let G_s be a spatial chain graph according to Definition 4 corresponding to \mathbf{X} with mutually disjoint sets $A_c \cup B_c \cup S_c \subseteq \mathbf{X}_c \subset \mathbf{X}$, where \mathbf{X}_c are the observations pertaining to crop c . Then, if S_c separates A_c and B_c in the spatial chain graph, we have that we have that

$$A_c \perp\!\!\!\perp B_c | S_c.$$

Proof. The vectors consisting of spatially filtered data \mathbf{E}_i are independently distributed as $N(\mathbf{0}, \Theta_E^{-1})$, $i = 1, \dots, n$, where information pertaining to within-crop relations for any crop c can be found in Θ_E . This property of independence conditional on a separating set is known as the global Markov property. Lauritzen (1996) provides a proof that any data arising from a multivariate normal distribution satisfy the global Markov property on its graph. \square

Given that the global Markov property holds for any crop in the spatial chain graph, the local and pairwise Markov properties hold as well (Lauritzen, 1996).

In line with the typical spatial autoregressive models that do not exhibit independence between non-first-order neighbours, we show that the proposed method does not either. Let the data generating process be $\text{vec}(\mathbf{X}) = \left(\mathbf{I}_{np} - \sum_{k=1}^2 \Psi_k^T \otimes \mathbf{W}_k \right)^{-1} \text{vec}(\mathbf{E})$. The inverse term is what causes dependencies between a location and its non-first-order neighbours through the residuals as $\left(\mathbf{I}_{np} - \sum_{k=1}^2 \Psi_k^T \otimes \mathbf{W}_k \right)^{-1} \text{vec}(\mathbf{E}) = \left[\mathbf{I}_{np} + \sum_{q=1}^{\infty} \left(\sum_{k=1}^2 \Psi_k^T \otimes \mathbf{W}_k \right)^q \right] \text{vec}(\mathbf{E})$, dependencies between a location and its non-first-order neighbours exist. Naturally, the first order term $\left(\sum_{k=1}^2 \Psi_k^T \otimes \mathbf{W}_k \right)^1$ results in a non-zero matrix, but so do the higher order terms, causing spillovers to non-neighbouring plots of the residual term \mathbf{E} . However, we have that $\left(\sum_{k=1}^2 \Psi_k^T \otimes \mathbf{W}_k \right)^q < \left(\sum_{k=1}^2 \Psi_k^T \otimes \mathbf{W}_k \right)^{q-1}$, with $q \in \{x \in \mathbb{N} | x > 1\}$, due to the restriction imposed by Assumption 1. This result implies that the strength of the spatial effect decreases as the neighbour order increases. The spillovers occur only within sequences of adjacent plots, not between sequences of adjacent plots. Empirically, the spillovers make sense: whilst most of the interaction between-plant happens between those that are adjacent to one another, it is impossible to guarantee complete isolation from non-adjacent plots, due to influences from weather (runoff, wind) or soil (percolation). Moreover, the further away plots are, the less strong the spatial effect. However, these spillovers happen only between crops that share at least 1 border on their respective plots. Due to identifiability issues, the proposed method cannot handle more than 2 crops. In spite of this, for trials containing more than 2 crops, crop combinations that do not share a border are independent, implying that the method can even handle data obtained from large-scale intercropping trials, as long as the combinations are analysed separately. This is shown in the following Theorem.

Theorem 2. (*Between-crop independence: non-neighbours*) Let $G_{s:c,c'}$ and $G_{s:c'',c'''}$ be spatial chain graphs according to Definition 4 corresponding to $\mathbf{X}_{c,c'}$ and $\mathbf{X}_{c'',c''''}$ respectively, such that $\mathbf{X}_{c,c'} \cup \mathbf{X}_{c'',c'''} \subseteq \mathbf{X}$, with disjoint sets $A_{c,c'} \subseteq \mathbf{X}_{c,c'}$ and $B_{c'',c'''} \subseteq \mathbf{X}_{c'',c''''}$, where $c' \in \mathcal{N}_c$ and $c'''' \in \mathcal{N}_{c''}$. Then, if $c, c' \notin \mathcal{N}_{c''} \cup \mathcal{N}_{c''''}$ we have that

$$A_{c,c'} \perp\!\!\!\perp B_{c'',c'''}.$$

Proof. Suppose for simplicity, and without loss of generality, that $\mathbf{X}_{c,c'} \cup \mathbf{X}_{c'',c'''} = \mathbf{X}$ and that $A_{c,c'}$ and $B_{c'',c''''}$ contain an equal number of observations n for a total number of $2n$ observations in \mathbf{X} . We can represent the spatial weight matrices for the observations pertaining to $A_{c,c'}$ as $\bar{\mathbf{W}}_{c,c'} = \begin{pmatrix} \mathbf{W}_{c,c'} & \mathbf{O}_n \\ \mathbf{O}_n & \mathbf{O}_n \end{pmatrix}$ and $\bar{\mathbf{W}}_{c',c} = \begin{pmatrix} \mathbf{W}_{c',c} & \mathbf{O}_n \\ \mathbf{O}_n & \mathbf{O}_n \end{pmatrix}$ and those of $B_{c'',c''''}$ as $\bar{\mathbf{W}}_{c'',c''''} = \begin{pmatrix} \mathbf{O}_n & \mathbf{O}_n \\ \mathbf{O}_n & \mathbf{W}_{c'',c''''} \end{pmatrix}$ and $\bar{\mathbf{W}}_{c''',c''} = \begin{pmatrix} \mathbf{O}_n & \mathbf{O}_n \\ \mathbf{O}_n & \mathbf{W}_{c''',c''} \end{pmatrix}$, with \mathbf{O}_n being a $n \times n$ zero matrix, where the various $\mathbf{W} \in \mathcal{Z}^{n \times n}$ are sub-neighbour matrices only containing locations with the crops stated in the subscript, and with the $\bar{\mathbf{W}} \in \mathcal{Z}^{2n \times 2n}$. Due to the block structure of the weight matrices, the spatial filter matrix $\mathbf{R}(\Psi)$ becomes separable for the Ψ_k , such that

$$\begin{aligned} & \left(\begin{array}{c} \left(\mathbf{I}_{2np} - \Psi_{c,c'}^T \otimes \bar{\mathbf{W}}_{c,c'} - \Psi_{c',c}^T \otimes \bar{\mathbf{W}}_{c',c} \right)^{-1}_{[c,c']} \\ \left(\mathbf{I}_{2np} - \Psi_{c'',c''''}^T \otimes \bar{\mathbf{W}}_{c'',c''''} - \Psi_{c''',c''}^T \otimes \bar{\mathbf{W}}_{c''',c''} \right)^{-1}_{[c'',c''']} \end{array} \right) \\ & = \left(\mathbf{I}_{2np} - \Psi_{c,c'}^T \otimes \bar{\mathbf{W}}_{c,c'} - \Psi_{c',c}^T \otimes \bar{\mathbf{W}}_{c',c} - \Psi_{c'',c''''}^T \otimes \bar{\mathbf{W}}_{c'',c''''} - \Psi_{c''',c''}^T \otimes \bar{\mathbf{W}}_{c''',c''} \right)^{-1}, \end{aligned}$$

where $[c, c']$ indicates the rows that pertain to observations of crops c and c' . Above result shows the independence of the data generating process of combinations c, c' and c'', c'''' and completes the proof. \square

The result from this theorem leads to the following special case for neighbouring crops.

Corollary 1. (*Between-crop independence: no spatial effect*) Let G_s be a spatial chain graph according to Definition 4 corresponding to \mathbf{X} with disjoint sets $A_c \subseteq \mathbf{X}_c$ and $B_{c'} \subseteq \mathbf{X}_{c'}$, such that $\mathbf{X}_c \cup \mathbf{X}_{c'} \subseteq \mathbf{X}$, where $c \neq c'$. Then, if $c' \in \mathcal{N}_c$ and $\Psi_{c',c} = \Psi_{c,c'} = \mathbf{O}_p$ we have that

$$A_c \perp\!\!\!\perp B_{c'}.$$

Proof. As the spatial effect matrices $\Psi_{c',c}$ and $\Psi_{c,c'}$ both equal \mathbf{O}_p , we have that the data generating process reduces to $\text{vec}(\mathbf{X}) = \text{vec}(\mathbf{E})$, indicating that the data depend only on the within-plot effects, thereby confirming the independence between any subsets of \mathbf{X}_c and $\mathbf{X}_{c'}$. \square

2.5 Identifiability

The popular adage “there is no such thing as a free lunch”, holds true even in statistics. Given that our model is highly parameterised, identification, and therefore estimation is a non-trivial issue, one that is not often considered in the Bayesian setting, as informative priors have the potential to circumvent identification issues. Whilst we agree that informative priors have their place in statistical inference, only relying on informative priors is too restrictive in our view as it turns the proposed method into a confirmatory method and does not allow for any exploratory analysis. To this end, we allow for both informative priors and parameter restrictions such that model identification, and in turn Bayesian learning, becomes possible which enables the method to be used in both exploratory and confirmatory analysis. In the proposed method, we have that the model is identifiable for Θ_E , but not for the various Ψ_k , without informative priors or additional parameter restrictions. To this end, the following parameter restrictions are proposed

Assumption 2. (*Identifiability restrictions*) *To identify the spatial effects, we impose the following restrictions on the various Ψ_k (i) $\psi_{kii} \sim N(0, \tau)$, for all $i = 1, \dots, p$, and for small $\tau > 0$ and (ii) $\Psi_k = \Psi_k^T$ or (iii) the Ψ_k are (near) triangular matrices where the 0-elements are assigned the same $N(0, \tau)$ priors as the diagonal. Alternatively, we can impose restriction (iv) where $N(0, \tau)$ priors are imposed on known 0-effects of the Ψ_k for $1 \leq k \leq 2$.*

Other informative priors can be imposed on the diagonal, if desired. Note that we require both restrictions (i) and (ii) or (i) and (iii) to obtain identifiability, as without these restrictions, or informative priors, regardless of the number of observations, the parameters cannot be estimated. However, restriction (iv) is sufficient for identifiability, provided there exists at least $p^2/2$ known 0-effects per Ψ_k . Whenever there exists an insufficient number of such effects, using tight nonzero priors on known positive or negative effects can aid in model identification. Consider intercropping data consisting of production (e.g. yield), environmental and management variables. Whilst management variables might affect production variables, it is a-priori known that the reverse direction contains no effect. This restriction makes optimal use of existing knowledge, whilst limiting biased estimates. It is up to the researcher to choose the appropriate restriction, which varies on a case-by-case basis.

As identification issues remain for trials with more than 2 crops, we recommend that the parameters corresponding to each crop combination are estimated separately from the other combinations by fitting a different model for each combination. The downside of this is that we cannot pool the observations to estimate the common precision matrix, but obtain different Θ_E for each combination, whose differences disappear asymptotically. As such, by Theorem 2, asymptotically, it is irrelevant for the Ψ_k whether they are estimated in a joint-fashion, or whether we estimate them separately for each combination. It is impossible to further generalize Theorem 2 to separately estimate the Ψ_k , thereby loosening the restrictions imposed in Assumption (2), as we have

$$\text{that } \begin{pmatrix} (\mathbf{I}_{np} - \Psi_{c,c'}^T \otimes \mathbf{W}_{c,c'})_{[c']}^{-1} \\ (\mathbf{I}_{np} - \Psi_{c',c}^T \otimes \mathbf{W}_{c',c})_{[c]}^{-1} \end{pmatrix} \neq (\mathbf{I}_{np} - \Psi_{c,c'}^T \otimes \mathbf{W}_{c,c'} - \Psi_{c',c}^T \otimes \mathbf{W}_{c',c})^{-1} \neq \begin{pmatrix} (\mathbf{I}_{np} - \Psi_{c,c'}^T \otimes \mathbf{W}_{c,c'})_{[c]}^{-1} \\ (\mathbf{I}_{np} - \Psi_{c',c}^T \otimes \mathbf{W}_{c',c})_{[c']}^{-1} \end{pmatrix},$$

$c' \in \mathcal{N}_c$, due to the interdependence between the two crops. Note that the $\begin{pmatrix} \cdot \\ \cdot \end{pmatrix}$ does not represent explicit matrix stacking as in Theorem 2, but rather a matrix where we stack the rows of the spatial filter matrices according to their location in the intercropping design.

3 Bayesian inference

A Bayesian framework for the spatial autoregressive model consists of two choices: the prior choice for the autoregressive parameters and the prior choice for the within-plot precision matrix. In fact, an additional consideration for the autoregressive parameters needs to be made: do we impose sparsity-inducing priors or not? Sparsity — having a majority of zero coefficients — has seen a surge of interest over the last few years, including in the spatial autoregressive literature (Pfarrhofer & Piribauer, 2019), and has various advantages over priors that result in non-sparse estimates, such as selecting only relevant variables in high-dimensional situations ($n \ll p$) for improved predictive accuracy, increased interpretability by forcing certain coefficients to zero and faster parameter estimation. To ensure that the proposed method is generalisable, we allow for both non-sparse and sparse spatial autoregressive priors. For the former, we choose the normal prior (LeSage & Chih, 2018) and for the latter the normal-gamma prior. The normal-gamma prior has shown good performance under conditions of (intermediate) sparsity (Huber & Feldkircher 2019; Kastner & Huber, 2020).

Even though elaborate prior structures are considered for the residual covariance matrix in the aforementioned articles, they are not applicable to the proposed model, as they do not lend themselves to structure learning of the within-plot effect graph. To learn the graph structure of a graphical model, researchers typically impose the conjugate G-Wishart prior on the precision matrix and assume a uniform or truncated Poisson on the graph space (Dawid & Lauritzen, 1993; Roverato, 2002; Mohammadi & Wit, 2015). However, unless a decomposable graph is assumed, which is atypical, this prior requires computationally intensive evaluation of a constant, which hinders generalisability to big or high-dimensional data. For this reason, Wang (2012) introduced the Bayesian graphical lasso; an efficient framework to perform Bayesian inference for the graphical lasso. An improvement of the Bayesian graphical lasso has recently been proposed by Li et al. (2019): the graphical horseshoe prior. This prior has shown excellent performance in graph structure learning, whilst remaining computationally efficient and will be our prior choice on Θ_E . Even though the horseshoe prior is known to be conservative in terms of variable selection (van der Pas et al., 2017), i.e. few true zero parameters in the model are falsely selected, whilst some of the true non-zero parameters are not selected, Li et al. (2019) mitigated the number of false negatives by using the 50% credible interval for variable selection. These priors are implemented in an efficient Gibbs sampling algorithm, that allows researchers to estimate the parameters corresponding to the spatial chain graph for small, moderate or large p in a reasonable amount of time. We will only illustrate the Gibbs sampler for the normal-gamma prior on the autoregressive parameters and not for the normal prior, as its implementation is trivial. Nonetheless, we will illustrate the performance of all priors in Section 4.

The first step of our Bayesian estimation procedure is the likelihood, which under the assumption of multivariate normality of the residuals in (2), is given by

$$P(\mathbf{X}|\Psi_1, \Psi_2, \Theta_E) = (2\pi)^{-\frac{np}{2}} \det(\Theta_E)^{\frac{n}{2}} \det[\mathbf{R}(\Psi)] \exp \left\{ -\frac{1}{2} [\mathbf{R}(\Psi) \text{vec}(\mathbf{X})]^T (\Theta_E \otimes \mathbf{I}_n) \mathbf{R}(\Psi) \text{vec}(\mathbf{X}) \right\} \\ \propto \det(\Theta_E)^{\frac{n}{2}} \det[\mathbf{R}(\Psi)] \exp \left[-\frac{1}{2} \text{tr}(\mathbf{S}\Theta_E) \right], \quad (3)$$

with $\mathbf{S} = \left(\mathbf{X} - \sum_{k=1}^2 \mathbf{W}_k \mathbf{X} \Psi_k \right)^T \left(\mathbf{X} - \sum_{k=1}^2 \mathbf{W}_k \mathbf{X} \Psi_k \right)$. Due to the formulation of the likelihood in (3), the block sampling algorithm of Li et al. (2019) is straightforwardly applied on the estimation of Θ_E when holding Ψ_1 and Ψ_2 constant. Horseshoe priors are imposed on the upper-triangular elements of the precision matrix (due to the symmetry of Θ_E), and a uniform prior on the diagonal elements. This results in the following element-wise hierarchical structure

$$\begin{aligned} \theta_{Eii} &\propto 1, \\ \theta_{Eij: i < j} &\sim N(0, \lambda_{ij}^2 \tau^2), \\ \lambda_{ij: i < j} &\sim C^+(0, 1), \\ \tau &\sim C^+(0, 1), \end{aligned}$$

where the global and local hyperparameters follow a half-Cauchy distribution. The full conditional posterior of Θ_E then has the following form

$$P(\Theta_E | \mathbf{X}, \Psi_1, \Psi_2, \Lambda, \tau) \propto \det(\Theta_E)^{\frac{n}{2}} \exp \left[-\frac{1}{2} \text{tr}(\mathbf{S}\Theta_E) \right] \prod_{i < j} \exp \left(-\frac{\theta_{Eij}^2}{2\lambda_{ij}^2 \tau^2} \right) \mathbb{I}_{\Theta_E \in \mathcal{M}_p^+},$$

where \mathbb{I} is an indicator function, $\Lambda = (\lambda_{ij}^2)$ and \mathcal{M}_p^+ is the space of $p \times p$ positive definite matrices. Sampling from this posterior is not straightforward, and Li et al. (2019) propose a modified version of the efficient block Gibbs sampler introduced in Wang (2012), whereby one column and row of Θ_E are updated at a time. We will not recapitulate the algorithm here, and interested readers are referred to the aforementioned articles.

Continuing with the autoregressive parameters, the normal-gamma global-local shrinkage prior leads to the following hierarchical structure

$$\begin{aligned} \psi_{kij} | \alpha_{kij} &\sim N(0, 2\omega^{-2} \alpha_{kij}), \\ \alpha_{kij} &\sim G(\kappa, \kappa), \\ \omega^2 &\sim G(c_0, c_1), \end{aligned}$$

for $1 \leq k \leq 2$ and $1 \leq i, j \leq p$, with local shrinkage parameter α_{kij} , global shrinkage parameter ω^2 and hyperparameters κ, c_0 and c_1 specified by the researcher. Observe that a-priori we assume independence of Θ_E and the Ψ_k . Both the local and global shrinkage parameters follow a Gamma distribution. Due to the hierarchical nature of these priors, the conditional posteriors are similar to those of the aforementioned articles, as the likelihood is not involved, except for the lowest level (that of the ψ_{kij}), for which no known distribution exists in our case given the presence of the $\det[\mathbf{R}(\Psi)]$ term. Therefore, we use a Metropolis-Hastings (MH) step

in the Gibbs sampler to sample from the full conditionals of ψ_{kij} . The conditional posteriors of the shrinkage parameters are

$$P(\alpha_{kij}|\psi_{kij}, \omega) \sim \text{GIG}\left(\kappa - \frac{1}{2}, \psi_{kij}^2, \kappa\omega^2\right),$$

$$P(\omega^2|\alpha_{111}, \dots, \alpha_{2pp}) \sim \text{G}\left(c_0 + \kappa 2p^2, c_1 + \frac{\kappa}{2} \sum_{k=1}^2 \sum_{i=1}^p \sum_{j=1}^p \alpha_{kij}\right),$$

such that the local shrinkage parameters follow a generalized inverse Gaussian distribution and the global shrinkage parameters follow a Gamma distribution. As stated above, to obtain the ψ_{kij} , we use a MH step within the Gibbs algorithm, where a new value ψ_{kij}^p is proposed $\psi_{kij}^p \sim N(\psi_{kij}^{(t-1)}, \zeta)$, with ζ being a tuning parameter to increase efficiency of the MH step. To avoid numerical underflow, we take the natural logarithm of the acceptance rate. If $\log [P(\mathbf{X}|\psi_{1ij}^p, \Theta_E^{(t)}, \Psi_{1-ij}^{(t-1)}, \Psi_2^{(t-1)})] + \log [P(\psi_{1ij}^p)] > \log [P(\mathbf{X}|\psi_{1ij}^{(t-1)}, \Theta_E^{(t)}, \Psi_{1-ij}^{(t-1)}, \Psi_2^{(t-1)})] + \log [P(\psi_{1ij}^{(t-1)})]$ set $\psi_{kij}^{(t)} = \psi_{kij}^p$ and set $\psi_{kij}^{(t)} = \psi_{kij}^{(t-1)}$ otherwise. The hyperparameters in the acceptance step are omitted and we set $k = 1$ to simplify the notation. Note that due to the separable nature of the priors on the individual spatial effect components, combined with the restrictions imposed by Assumption 2, we end up with respectively $p(p+1)$, $2p^2$ and $2p^2$ MH steps for identifiability restrictions (ii), (iii) and (iv) within each iteration of the Gibbs sampling procedure. To guarantee the stability condition imposed on the spatial effects, see Assumption (1), we redraw values for ψ_{kij}^p until the condition is met.

4 Simulation study

To illustrate the performance of the proposed methodology on data of different dimensionality and network structure, a simulation study was conducted. Whilst competing models do not exist, the relevance of this study is found in its capacity to shed light on the adequacy of Bayesian learning of the true parameters underlying the proposed method.

The three network structures that underlie Θ_E for the simulation study are random, scale-free and star. Whilst our main interest is illustrating to what extend the Gibbs method can estimate the Ψ_k , multiple networks underlying Θ_E were chosen to represent various types of dependence relations, thereby illustrating the versatility of the proposed method.

For each network structure, 20 spatial autoregressive graphical models are fitted for trials consisting of 2 crops, with $n \in \{25, 50, 100\}$ and $p \in \{4, 8\}$. We showcase model performance using restrictions (i), (ii) and (iii) of Assumption 2, where we set all Ψ_k to be upper triangular for models adhering to restriction (iii). We do not evaluate the performance of the method with restriction (iv), as it is a generalisation of restriction (iii). The dimensionality of simulated data is consistent with the data commonly found in intercropping designs.

The discrepancy between the true and the estimated parameters are measured using the Frobenius norm, $\|\Theta_E^0 - \hat{\Theta}_E\|_F$ for Θ_E and the mean absolute error $\frac{1}{2p^2} \sum_{k=1}^2 \sum_{i=1}^p \sum_{j=1}^p |\psi_{kij}^0 - \hat{\psi}_{kij}|$ and the root mean square error $\sqrt{\frac{1}{2p^2} \sum_{k=1}^2 \sum_{i=1}^p \sum_{j=1}^p (\psi_{kij}^0 - \hat{\psi}_{kij})^2}$ for the Ψ_k , where the discrepancy measures are averaged over the 20 fitted models.

The data is simulated by first constructing Θ_E according to the chosen network type, followed by independently drawing the residual vectors $\mathbf{E}_i \sim N_p(\mathbf{0}, \Theta_E^{-1})$ for $i = 1, \dots, n$. Under assumptions of sparsity, i.e. the simulations where normal-gamma priors are used, for each $k \in \{1, 2\}$ we draw $p-1$ elements from a $U(-1, 1)$ distribution, and randomly assign these to spatial effects ψ_{kij} , whilst setting all other $p(p-1)+1$ elements to zero. When normal priors are used, we draw spatial effects $\psi_{kij} \sim U(-1, 1)$ for all k, i, j . For both priors, the spatial effects are subsequently transformed to adhere to restriction (i) by drawing $\psi_{kii} \sim N(0, \tau)$ as well as either restriction (ii) or restriction (iii) from Assumption 2. Finally, we set $\text{vec}(\mathbf{X}) = (\mathbf{I}_{np} - \sum_{k=1}^2 \Psi_k^T \otimes \mathbf{W}_k)^{-1} \text{vec}(\mathbf{E})$. For each parameter combination, we use the first 1000 iterations as burn-in from a total of 2000 iterations. Inference is based on the 1000 posterior draws for all parameters, where we use the posterior mean as a point estimate to compute the Frobenius norm, mean absolute error and root mean squared error. The results for the simulation study can be found in Table 1 where normal priors are implemented with hyperparameters $\mu = 0, \sigma = 1$ and in Table 2 using normal-gamma priors with hyperparameters $c_0 = c_1 = 0.01$ and $\kappa = 0.1$ (Huber & Feldkircher, 2019; Pfarrhofer & Piribauer, 2019). For parameter restrictions (i) and (iii), we fix $\tau = 0.001$.

Table 1: Simulation results for the random, scale-free and star networks, using the normal prior for both symmetric and triangular parameter restrictions. FN stands for Frobenius norm, MAE stands for mean absolute error and RMSE stands for root mean square error. The discrepancy measures are averaged across 20 fitted models for each parameter combination and rounded to 2 decimals. Standard errors are provided between parentheses.

Random network		Symmetric restriction			Triangular restriction		
n, p		FN	MAE	RMSE	FN	MAE	RMSE
25, 4		2.60 (0.62)	0.20 (0.03)	0.28 (0.03)	2.51 (0.57)	0.11 (0.01)	0.22 (0.02)
50, 4		0.89 (0.12)	0.13 (0.01)	0.18 (0.02)	0.75 (0.06)	0.07 (0.00)	0.15 (0.01)
100, 4		0.89 (0.17)	0.11 (0.01)	0.15 (0.02)	0.70 (0.10)	0.06 (0.00)	0.11 (0.01)
25, 8		9.03 (1.21)	0.23 (0.02)	0.31 (0.02)	11.17 (3.80)	0.14 (0.00)	0.27 (0.01)
50, 8		6.34 (1.91)	0.17 (0.01)	0.23 (0.02)	3.35 (1.00)	0.10 (0.00)	0.19 (0.01)
100, 8		4.10 (1.12)	0.16 (0.02)	0.21 (0.02)	2.29 (1.01)	0.07 (0.00)	0.13 (0.00)
Scale-free network							
25, 4		2.38 (0.34)	0.20 (0.02)	0.28 (0.03)	2.21 (0.39)	0.11 (0.01)	0.23 (0.01)
50, 4		1.26 (0.21)	0.16 (0.02)	0.23 (0.02)	1.09 (0.13)	0.08 (0.01)	0.16 (0.01)
100, 4		1.06 (0.20)	0.11 (0.01)	0.15 (0.02)	0.74 (0.10)	0.06 (0.00)	0.12 (0.01)
25, 8		10.89 (1.85)	0.23 (0.02)	0.31 (0.02)	12.34 (2.84)	0.15 (0.00)	0.29 (0.01)
50, 8		6.02 (1.45)	0.18 (0.01)	0.25 (0.02)	5.03 (1.50)	0.10 (0.00)	0.19 (0.01)
100, 8		4.90 (1.97)	0.14 (0.02)	0.19 (0.02)	1.61 (0.32)	0.07 (0.00)	0.13 (0.00)
Star network							
25, 4		2.36 (0.23)	0.22 (0.02)	0.30 (0.03)	2.98 (0.67)	0.11 (0.01)	0.22 (0.01)
50, 4		1.24 (0.20)	0.15 (0.02)	0.20 (0.03)	1.28 (0.24)	0.08 (0.01)	0.15 (0.01)
100, 4		0.95 (0.11)	0.11 (0.01)	0.15 (0.01)	0.98 (0.14)	0.06 (0.00)	0.11 (0.01)
25, 8		12.01 (3.26)	0.22 (0.01)	0.31 (0.02)	13.52 (3.64)	0.15 (0.01)	0.29 (0.01)
50, 8		5.70 (1.44)	0.17 (0.01)	0.23 (0.01)	4.95 (1.45)	0.10 (0.00)	0.19 (0.01)
100, 8		3.39 (0.66)	0.15 (0.02)	0.19 (0.02)	2.70 (0.76)	0.07 (0.00)	0.13 (0.00)

Table 2: Simulation results for the random, scale-free and star networks, using the normal-gamma prior for both symmetric and triangular parameter restrictions. FN stands for Frobenius norm, MAE stands for mean absolute error and RMSE stands for root mean square error. The discrepancy measures are averaged across 20 fitted models for each parameter combination and rounded to 2 decimals. Standard errors are provided between parentheses.

Random network		Symmetric restriction			Triangular restriction		
n, p		FN	MAE	RMSE	FN	MAE	RMSE
25, 4		1.75 (0.21)	0.23 (0.02)	0.34 (0.04)	1.60 (0.19)	0.14 (0.01)	0.28 (0.02)
50, 4		1.00 (0.13)	0.16 (0.02)	0.23 (0.03)	0.74 (0.09)	0.09 (0.01)	0.17 (0.01)
100, 4		0.76 (0.09)	0.12 (0.01)	0.16 (0.02)	0.53 (0.06)	0.07 (0.00)	0.13 (0.01)
25, 8		9.53 (2.51)	0.30 (0.03)	0.41 (0.04)	8.84 (2.12)	0.17 (0.01)	0.34 (0.02)
50, 8		5.30 (1.72)	0.24 (0.02)	0.32 (0.02)	3.02 (0.50)	0.11 (0.01)	0.21 (0.01)
100, 8		3.24 (0.90)	0.16 (0.02)	0.22 (0.02)	1.35 (0.16)	0.07 (0.00)	0.14 (0.01)
Scale-free network							
25, 4		2.85 (0.49)	0.21 (0.02)	0.29 (0.03)	1.79 (0.17)	0.14 (0.01)	0.27 (0.01)
50, 4		1.78 (0.37)	0.16 (0.02)	0.21 (0.02)	0.84 (0.10)	0.09 (0.01)	0.18 (0.01)
100, 4		1.70 (0.60)	0.11 (0.02)	0.15 (0.02)	0.81 (0.11)	0.06 (0.00)	0.13 (0.01)
25, 8		9.88 (4.10)	0.30 (0.01)	0.42 (0.02)	9.94 (1.61)	0.20 (0.01)	0.38 (0.02)
50, 8		7.40 (4.13)	0.22 (0.02)	0.30 (0.02)	3.95 (1.12)	0.12 (0.00)	0.24 (0.01)
100, 8		7.59 (4.53)	0.16 (0.02)	0.22 (0.03)	2.19 (0.41)	0.08 (0.00)	0.15 (0.01)
Star network							
25, 4		2.37 (0.33)	0.24 (0.03)	0.36 (0.04)	3.58 (0.95)	0.13 (0.01)	0.26 (0.02)
50, 4		1.10 (0.14)	0.17 (0.02)	0.24 (0.02)	1.14 (0.13)	0.09 (0.01)	0.18 (0.01)
100, 4		0.70 (0.11)	0.12 (0.02)	0.17 (0.03)	0.87 (0.08)	0.07 (0.00)	0.14 (0.01)
25, 8		6.05 (1.19)	0.33 (0.02)	0.44 (0.03)	8.58 (1.43)	0.20 (0.01)	0.4 (0.03)
50, 8		3.07 (0.32)	0.22 (0.01)	0.30 (0.02)	3.82 (0.88)	0.11 (0.01)	0.22 (0.01)
100, 8		2.17 (0.27)	0.18 (0.02)	0.24 (0.02)	1.77 (0.38)	0.07 (0.00)	0.14 (0.01)

As observed in Tables 1 and 2, for all network types, prior assumptions, identifiability restrictions and number of parameters, the discrepancy measures for posterior mean point estimates reduce as the sample size of the data grows. Whilst the estimation accuracy of the method appears invariant to the underlying network structure, it is not invariant to the identifiability restriction. This result is not particularly remarkable, considering that under the triangular restriction, the lower triangular estimates of the Ψ_k contribute next to nothing to the discrepancy measures, whilst under a symmetric restriction these elements contribute equally to the discrepancy measures as the upper triangular elements do. Finally, both priors show satisfactory and similar performance.

5 Real world data example

We have primarily motivated the present model through an intercropping framework, begging a demonstration on actual intercropping data. The included example consists of a paired-crop type design of Belgian endive and beetroot, where each plot, consisting of multiple plants, has a single neighbour of the other species. Although three distinct genotypes were used for each crop, we assume homogeneity between these genotypes in terms of spatial effects for this analysis, as the sample size would be insufficient to obtain meaningful parameter estimates otherwise. Belgian endive can be found to the right of beetroot 4 times and 5 times to the left, resulting in a total of 18 observations. The design is shown in Figure 1, which also contains the variable values for the plots. The variables in this dataset are plant weight, plant height and number of plants, where the first two variables are averaged across all plants within a plot. Whilst the position of the crop, left or right, has potential consequences for the spatial effects, for this application we assume that the spatial effects are homogeneous, regardless of whether a crop is to the left, or to the right of its neighbour. Given the borders between each pair of observations, no spatial spillovers are expected to occur between non-neighbouring plots. Therefore, each pair of Belgian endive and beetroot is independent of all other pairs. The data used in this study was generated through the strategic investment theme ‘Biodiversity-positive Food Systems’ of Wageningen University & Research.

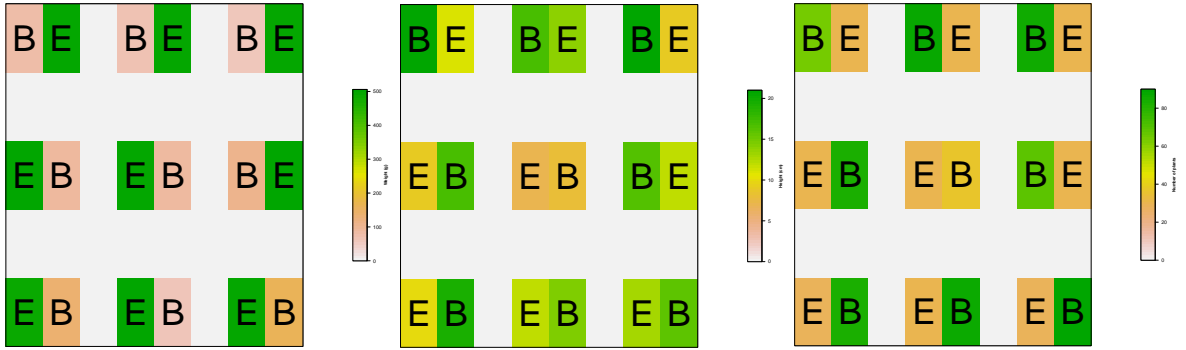


Figure 1: Paired crop intercropping design with two different crops: Belgian endive (E) and beetroot (B). Variable values for the weight, height and number of plants are illustrated by colours.

Whilst the plots containing Belgian endive typically contain more biomass in terms of weight than those containing beetroot, the number of plants per plot, as well as the average plant height tend to be higher for beetroot.

We use the following equation to represent the stochastic model underlying the observed data

$$\mathbf{X} = \mathbf{W}_{B,E}\mathbf{X}\Psi_{B,E} + \mathbf{W}_{E,B}\mathbf{X}\Psi_{E,B} + \mathbf{E}, \quad \mathbf{E}_i \sim N_p(\mathbf{0}, \Theta_E^{-1}), \quad i = 1, \dots, 18.$$

Given that all variables in the data are a representation of plant biomass, we impose symmetric restrictions on $\Psi_{B,E}$ and $\Psi_{E,B}$, as we expect relations amongst biomass variables to be self-reinforcing, with the possible exception for the number of plants, due to the additional competition that arises from more plants per plot. In addition, we assume normal priors for the spatial effects, as there is no a-priori reason to assume that there exists no spatial influences of these biomass variables. In addition, given that the dimensionality of the data is low, there is no need for additional interpretability through sparsity. We run the Gibbs sampling algorithm with a burnin of 5000, for 10000 total iterations. Diagnostic plots for the spatial effects are given in Figure 2, whilst the spatial chain graph is shown in Figure 3.

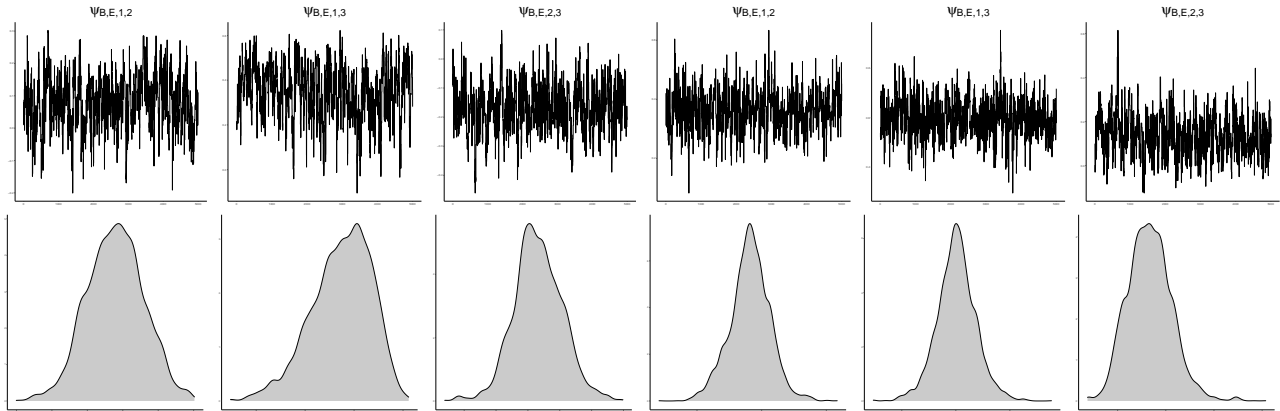


Figure 2: MCMC trace plots and posterior distributions.

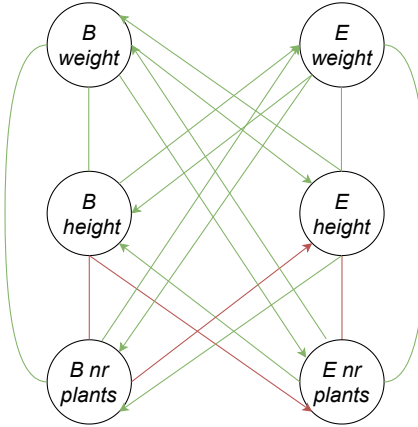


Figure 3: Spatial chain graph, based on the posterior means from Θ_E , $\Psi_{B,E}$ and $\Psi_{E,B}$, with positive (—) and negative effects (—).

Whilst the majority of the between- and within-plot effects are positive, there is a negative relationship between number of plants and height, with these traits in beetroot negatively affecting those in Belgian endive. A possible explanation for this result is that as the number of plants within a plot increases, competition for resources between plants in the plot increases as well, leading to less biomass (height) per plant. However, no negative within-plot effect between plant weight and the number of plants is found, contradicting the competition argument, unless the additional biomass obtained by having more plants offsets the loss of biomass due to shorter plants as a consequence of the increased competition. It appears that beetroot and Belgian endive exhibit both synergy and competition, judged by the respectively positive and negative spatial effects. One such synergistic spatial interaction is the one between weight and the number of plants. This interaction effect is the strongest interaction by magnitude (see Figure 2) and could hint at latent ecological relations. Moreover, the fitted model illustrates the need for asymmetric spatial effects for the crops, as not only the posterior means for the Ψ_k differ, but also the sign of the relations between plant height and the number of plants. In order to gain more insight into the exact nature of these synergistic and competitive effects, a second, more thorough analysis is needed, consisting of data with more variables that influence plant production, such as biological characteristics of the plant, e.g. root length and leaf area, as well as soil properties and management techniques to advance intercropping research.

6 Conclusion and discussion

In this contribution, we propose a new statistical methodology that is able to infer multivariate local and asymmetric spatial effects. In essence, the proposed model can be seen as a fusion, and extension, of two different models: the multivariate spatial autoregressive model and the Gaussian graphical model. By exploiting the flexibility offered by the spatial weight matrices, asymmetry in spatial effects is accounted for. As this results in a highly parameterised model, identifiability restrictions are imposed on the spatial effect matrices. The inferred local and spatial effects are represented by means of a graphical framework, facilitating interpretability. Bayesian learning is shown by means of a simulation study, where accurate point estimates are obtained for a variety of network structures.

One recommendation for future research is to allow for a different precision matrix for each crop. In some cases the assumption of homogeneous within-plot effects might be overly restrictive. On the flip side, removing such a restriction would greatly increase the computation time of the method, making it unattractive for datasets consisting of more observations and variables.

A downside of the method is the restrictiveness of the identifiability assumptions. These assumptions rely on prior knowledge of the underlying crop growth process. The question that arises is that if such prior knowledge exists, why use this method to begin with? The answer is that the proposed method provides numerical values and uncertainty pertaining to the values of these effects, which goes above and beyond typical prior knowledge. In addition, only knowledge of the zero-effects is sufficient to identify the model. The incorporation of prior knowledge or intuition in statistical methods can lead to discoveries that are otherwise unattainable. Moreover, researchers are not necessarily “restricted” to the set of identifiability restrictions proposed in this article. There exist other possible identification restrictions, which might be more suited to particular research questions or settings.

Acknowledgements

The authors would like to thank Anna Edlinger, Jan Peter van der Hoeve, Peter Bourke and Piter Bijma (Wageningen University & Research) for sharing the data. Generation of the data was supported by the Dutch Ministry of Agriculture, Nature and Food Quality (KB44-001-001).

References

Abegaz, F. and E. Wit (2013). Sparse time series chain graphical models for reconstructing genetic networks. *Biostatistics* 14(3), 586–599.

Barigozzi, M. and C. Brownlees (2019). Nets: Network estimation for time series. *Journal of Applied Econometrics* 34(3), 347–364.

Bourke, P. M., J. B. Evers, P. Bijma, D. F. van Apeldoorn, M. J. Smulders, T. W. Kuyper, L. Mommer, and G. Bonnema (2021). Breeding beyond monoculture: putting the “intercrop” into crops. *Frontiers in Plant Science* 12, 734167.

Brooker, R. W., A. E. Bennett, W.-F. Cong, T. J. Daniell, T. S. George, P. D. Hallett, C. Hawes, P. P. Iannetta, H. G. Jones, A. J. Karley, et al. (2015). Improving intercropping: a synthesis of research in agronomy, plant physiology and ecology. *New Phytologist* 206(1), 107–117.

Chu, G., Q. Shen, and J. Cao (2004). Nitrogen fixation and n transfer from peanut to rice cultivated in aerobic soil in an intercropping system and its effect on soil n fertility. *Plant and Soil* 263, 17–27.

Dahlhaus, R. and M. Eichler (2003). Causality and graphical models in time series analysis. *Oxford Statistical Science Series*, 115–137.

Dallakyan, A., R. Kim, and M. Pourahmadi (2022). Time series graphical lasso and sparse var estimation. *Computational Statistics & Data Analysis* 176, 107557.

Dawid, A. P. and S. L. Lauritzen (1993). Hyper markov laws in the statistical analysis of decomposable graphical models. *The Annals of Statistics*, 1272–1317.

Dobra, A. (2016). Graphical modeling of spatial health data. In *Handbook of Spatial Epidemiology*, pp. 593–612. Chapman and Hall/CRC.

Dobra, A., A. Lenkoski, and A. Rodriguez (2011). Bayesian inference for general gaussian graphical models with application to multivariate lattice data. *Journal of the American Statistical Association* 106(496), 1418–1433.

Federer, W. T. (2012). *Statistical design and analysis for intercropping experiments: Volume 1: Two crops*. Springer Science & Business Media.

Fordham, R. (1983). Intercropping—what are the advantages? *Outlook on Agriculture* 12(3), 142–146.

Gao, D., X. Pan, M. Khashi u Rahman, X. Zhou, and F. Wu (2021). Common mycorrhizal networks benefit to the asymmetric interspecific facilitation via k exchange in an agricultural intercropping system. *Biology and Fertility of Soils* 57(7), 959–971.

Getis, A. (1990). Screening for spatial dependence in regression analysis. In *Papers of the Regional Science Association*, Volume 69, pp. 69–81. Springer.

Homulle, Z., T. S. George, and A. J. Karley (2021). Root traits with team benefits: understanding belowground interactions in intercropping systems. *Plant and Soil*, 1–26.

Huang, C., Q. Liu, F. Gou, X. Li, C. Zhang, W. van der Werf, and F. Zhang (2017). Plant growth patterns in a tripartite strip relay intercrop are shaped by asymmetric aboveground competition. *Field Crops Research* 201, 41–51.

Huber, F. and M. Feldkircher (2019). Adaptive shrinkage in bayesian vector autoregressive models. *Journal of Business & Economic Statistics* 37(1), 27–39.

Kastner, G. and F. Huber (2020). Sparse bayesian vector autoregressions in huge dimensions. *Journal of Forecasting* 39(7), 1142–1165.

Lauritzen, S. L. (1996). *Graphical models*, Volume 17. Clarendon Press.

LeSage, J. P. and Y.-Y. Chih (2018). A bayesian spatial panel model with heterogeneous coefficients. *Regional Science and Urban Economics* 72, 58–73.

Li, C., T.-J. Stomph, D. Makowski, H. Li, C. Zhang, F. Zhang, and W. van der Werf (2023). The productive performance of intercropping. *Proceedings of the National Academy of Sciences* 120(2), e2201886120.

Li, Y., B. A. Craig, and A. Bhadra (2019). The graphical horseshoe estimator for inverse covariance matrices. *Journal of Computational and Graphical Statistics* 28(3), 747–757.

Long, D. S. (1998). Spatial autoregression modeling of site-specific wheat yield. *Geoderma* 85(2-3), 181–197.

Maitra, S., A. Hossain, M. Brešić, M. Skalicky, P. Ondrisik, H. Gitari, K. Brahmachari, T. Shankar, P. Bhadra, J. B. Palai, et al. (2021). Intercropping—a low input agricultural strategy for food and environmental security. *Agronomy* 11(2), 343.

Millo, G. (2014). Maximum likelihood estimation of spatially and serially correlated panels with random effects. *Computational Statistics & Data Analysis* 71, 914–933.

Mohammadi, A. and E. C. Wit (2015). Bayesian structure learning in sparse gaussian graphical models.

Ord, K. (1975). Estimation methods for models of spatial interaction. *Journal of the American Statistical Association* 70(349), 120–126.

Paci, L. and G. Consonni (2020). Structural learning of contemporaneous dependencies in graphical var models. *Computational Statistics & Data Analysis* 144, 106880.

Pfarrhofer, M. and P. Piribauer (2019). Flexible shrinkage in high-dimensional bayesian spatial autoregressive models. *Spatial statistics* 29, 109–128.

Roverato, A. (2002). Hyper inverse wishart distribution for non-decomposable graphs and its application to bayesian inference for gaussian graphical models. *Scandinavian Journal of Statistics* 29(3), 391–411.

Stern, W. (1993). Nitrogen fixation and transfer in intercrop systems. *Field crops research* 34(3-4), 335–356.

van der Pas, S., B. Szabó, and A. van der Vaart (2017). Uncertainty quantification for the horseshoe (with discussion). *Bayesian Analysis* 12(4), 1221–1274.

Wang, H. (2012). Bayesian graphical lasso models and efficient posterior computation. *Bayesian Analysis* 7(4), 867–886.

Yang, F., D. Liao, X. Wu, R. Gao, Y. Fan, M. A. Raza, X. Wang, T. Yong, W. Liu, J. Liu, et al. (2017). Effect of aboveground and belowground interactions on the intercrop yields in maize-soybean relay intercropping systems. *Field Crops Research* 203, 16–23.

Yang, J. and J. Peng (2020). Estimating time-varying graphical models. *Journal of Computational and Graphical Statistics* 29(1), 191–202.

Yang, K. and L.-f. Lee (2017). Identification and qml estimation of multivariate and simultaneous equations spatial autoregressive models. *Journal of Econometrics* 196(1), 196–214.

Zhang, W.-P., G.-C. Liu, J.-H. Sun, D. Fornara, L.-Z. Zhang, F.-F. Zhang, and L. Li (2017). Temporal dynamics of nutrient uptake by neighbouring plant species: evidence from intercropping. *Functional Ecology* 31(2), 469–479.